6610 *Biochemistry* **2009,** *48,* 6610–6617
DOI: 10.1021/bi900540j

BIOCHEMISTRY
including biophysical chemistry & molecular biology
Article

Delineating the Conformational Elements Responsible for Cu^{2+}-Induced Oligomerization of β-2 Microglobulin[†]

Dorottya V. Blaho and Andrew D. Miranker*

Department of Molecular Biophysics and Biochemistry Yale University, 260 Whitney Avenue, New Haven, Connecticut 06520-8114

Received March 30, 2009; Revised Manuscript Received June 10, 2009

ABSTRACT: β-2 microglobulin (β2m) is a small globular protein implicated in amyloid fiber formation in renal patients on long-term hemodialysis therapy. *In vitro*, under physiological conditions, β2m is not aggregation prone. However, in the presence of stoichiometric Cu^{2+}, β2m readily self-associates ultimately leading to heterogeneously sized aggregates. As this process occurs under near physiological solution conditions where the fold is ≥20 kJ/mol stabilized over the unfolded state, local conformational rearrangements are critical to understanding the oligomerization of β2m. The isomerization of a conserved *cis* proline at residue 32 is a recognized step in this process that can be initiated by Cu^{2+} binding. To better understand the structural basis of metal-induced oligomerization of β2m, we set out to determine the role of individual imidazole side chains in mediating metal binding affinity, native state stability, and oligomerization in the framework of P32A β2m. We find that P32A in the presence of Cu^{2+} forms a tetramer in an apparently cooperative manner. One interface of this tetramer appears to reside along an edge strand as H51 is a key residue in mediating oligomerization. Furthermore, H31 is the main Cu^{2+} binding residue in P32A and has an important role in stabilizing the protein in its holo form. Importantly, Cu^{2+} binding affinity in P32A is much greater than in WT. Here, we show that this strong binding affinity need not be directly coupled to oligomerization. We interpret our results in terms of the known structures of $\beta 2m_{apo}$ and a reversible hexameric state of $\beta 2m_{holo}$.

Amyloid and amyloid-like fibers are highly ordered protein aggregates that are associated with many diseases, including Alzheimer's, Parkinson's, and type II diabetes (*1*−*3*). Fibers result from the homomeric, noncovalent self-assembly of a normally soluble protein. The structure of such fibers is well-defined: β-strands form β-sheets that run parallel to the long axis of the fiber (*4*). Under the appropriate conditions, virtually any protein can form amyloid *in vitro* (*5*). Such conditions are quite varied and specific for a given system. In the case of a medically relevant system such as α-synuclein in Parkinson's Disease, these conditions are near physiological. In contrast, model systems such as myoglobin polymerize in response to heat and elevated pH (*6*). The challenge in the field is a determination of the mechanisms by which normally soluble states becomes aggregation prone.

Fiber formation may be treated like any other chemical reaction. Characterization of the mechanism therefore consists of elucidating the structures and energetics of intermediate states. In amyloid formation, this can have additional significance, as it is these intermediates that are generally associated with cytotoxicity in disease. For some systems, the precursor is globular, WT, and folded. This includes muscle acylphosphatase, transthyretin, lysozyme, and β-2 microglobulin (β2m) (*7*). Such systems represent a subclass of amyloid formation in which the protein adopts the amyloid state in response to an allosterically controlled conformational change. Alterations result in complementary surfaces that self-associate ultimately forming an irreversible state. It remains unclear why and how such alterations give rise to a specific amyloid structure.

β2m is a 12 kDa β-sandwich protein with an immunoglobulin fold. It forms the light chain of the class I Major Histocompatibility Complex (MHC) (*8*). In healthy individuals, turnover results in the release of β2m to the bloodstream followed by degradation mediated, in part, by the kidneys. For patients suffering from kidney failure treated by long-term hemodialysis, β2m forms amyloid fibers that deposit principally in the joints. Dialysis related amyloidosis (DRA)[1] is a condition that uniquely afflicts such patients in part because β2m is no longer properly catabolized (*9*, *10*). This results in a ∼10-fold elevation of the circulating protein (*9*, *11*). The higher concentration of β2m observed in DRA may be necessary but is not sufficient to induce amyloid formation. There are several other diseases, such as hepatitis C and leukemia, in which β2m levels are elevated, but there is no evidence of fiber formation (*12*, *13*). *In vivo*, β2m

[†]This work was supported by NIH DK54899.
*Author to whom correspondence should be addressed. Voice: (203) 432-8954. Fax: (203) 432-5175. E-mail: andrew.miranker@yale.edu.

[1]Abbreviations: AEW, average emission wavelength; AUC_{eq}, sedimentation equilibrium analytical ultracentrifugation; AUC_{sv}, sedimentation velocity analytical ultracentrifugation; DRA, dialysis related amyloidosis; HPLC, high performance liquid chromatography; PDB, protein data bank; rmsd, root-mean-square deviation; SEC, size exclusion chromatography; ThT, thioflavin T; β2m, β-2 microglobulin.

 Published on Web 06/11/2009

circulates at ~ 0.1 μM (*9*); however, *in vitro*, β2m is soluble and stable at near millimolar concentrations (*14*, *15*) and can be reversibly folded (*16*−*18*). Thus, under physiological conditions, β2m can be described as a well-behaved globular protein. A number of research efforts have resulted in conditions that enable *in vitro* amyloid formation to occur. This includes partial denaturation via diminished pH (*19*), proteolysis (*20*), SDS (*21*), TFE (*22*), and heat (*23*). Under physiological conditions, β2m has been induced to form amyloid by inclusion of serum proteins (*24*), nanoparticulates (*25*), and divalent cations (*14*, *26*). Our own work has focused on our discovery that β2m is a Cu^{2+} binding protein (*14*). In contrast to $\beta2m_{apo}$, $\beta2m_{holo}$ is aggregation prone under conditions comparable to human serum. Metal based allostery in amyloid represents an important class of amyloid mechanism that has been suggested to play a role in Alzheimer's, Parkinson's (*27*), and spongiform encephalopathies (*28*).

The addition of near stoichiometric amounts of Cu^{2+} to WT β2m results in the formation of species that while not amyloid, test positive for amyloid using the fluorescent indicator dye, thioflavin T (ThT) (*29*). These species arise on the hour time scale and are heterogeneously sized oligomers formed from dimeric subunits. Through mutagenesis and choice of solution conditions, sufficiently homogeneous populations can be isolated such that opportunities for atomic resolution structural studies have been possible (*30*). Importantly, these species do not appear to be amyloid nuclei. Rather, they represent lower energy states which contain an informative subset of the alterations required for subsequent and irreversible assembly. The initial formation of these oligomers is rate limited by a unimolecular rearrangement that can be catalyzed by Cu^{2+} binding (*29*). The binding site itself was shown by NMR (*31*), mutagenesis (*32*), mass spectrometry (*33*), and crystallographic studies (*30*) to involve the imidazole side chain of His 31. This is of particular interest as it is proximal to a conserved *cis* proline at residue 32.

The critical importance of the proline at residue 32 has been noted by several groups (*16*, *18*, *34*). The refolding of β2m includes a slow (~ 0.3 h^{-1}) step that has been attributed to isomerization of P32 (*18*). These authors hypothesized that the slow refolding step is caused by the *trans* to *cis* isomerization of P32 and that this contributes to the capacity of β2m to form amyloid. In kinetic analyses of fiber elongation at neutral pH, global analysis was used to suggest that this *trans* state was elongation competent (*16*). This finding was supported by the behavior of P32G which enhances the rate of fiber elongation and yields large amounts of amyloid fibers relative to WT β2m in the elongation assay. Indeed, the latter group has recently shown that fibers formed *in vitro* from P32G/I7A are spectroscopically comparable to *ex vivo* derived fibers (*35*).

In our own work, we have shown that the oligomerization profile and Cu^{2+} binding affinity of P32A is drastically changed compared to the WT protein (*34*). Under matched conditions, P32A oligomerizes much more rapidly and to a greater extent than WT. The affinity of P32A for Cu^{2+} is also dramatically increased. Whereas the binding affinity of WT protein for Cu^{2+} is ~3 μM, the Cu^{2+} binding affinity of P32A is ~0.5 nM. The crystal structure of $P32A_{apo}$ reveals several important features (*34*). Residue 32 is *trans*, a distal β-strand that contains a β-bulge in the WT protein has been rendered continuous, and the hydrophobic core of the protein is repacked giving P32A a more amphipathic character. These changes suggest that the imposition of an alternative conformation at residue 32 using a non-prolyl mutant results in an aggregation process in which the protein is predisposed to bypass some of the early steps. Here, we further investigate the properties of P32A that give rise to its aggregation prone state. The metal binding and oligomerization properties of P32A are characterized by mutagenesis of the four imidazole groups of the protein. This enables us to map the energies and specificities of cation-induced allostery that results in oligomerization.

EXPERIMENTAL PROCEDURES

Chemicals. Buffers and salts were obtained from Sigma Aldrich, J. T. Baker, and American Bioanalytical. Cloning and expression cell lines were obtained from Stratagene and Novagen, respectively.

Protein Expression. Mutants were made using the QuikChange Site Directed Mutagenesis kit (Stratagene) and confirmed by sequencing (Keck Facility, Yale University). Protein was expressed as previously described (*32*) but using a pET Blue2 plasmid and 6 h induction. Protein purity was assessed by SDS−PAGE and electrospray ionization mass spectrometry on a Micromass Platform LCT. The oxidation state of the internal disulfide in the protein was determined by reverse phase HPLC (*32*). The overall structure of mutants was analyzed by near UV-CD and found to be similar (Supporting Information, Figure 2). The mutants analyzed in this work are P32A, H13FP32A, H13AP32A, H31AP32A, H51FP32A, H51YP32A, H51AP32A, and H84AP32A. All P32A histidine double mutants are referred to by their histidine mutation. For instance, H51FP32A is simply H51F. The only caveat to this rule occurs in the discussion section, where $H13F_{holo}^{WT}$ refers to a previously studied mutant in which only H13 and not P32 is mutated (*30*).

Oligomerization. Oligomerization reactions were performed at 37 °C with 100 μM protein and 200 μM Cu^{2+} or 10 mM EDTA in 25 mM MOPS, 200 mM potassium acetate, and 500 mM urea at pH 7.4. All reaction components were pre-equilibrated at 37 °C and returned to 37 °C after mixing. The kinetics of oligomerization were monitored via the change in fluorescence of a histological dye, thioflavin T (ThT) (*36*). Samples were excited at 440 nm and emission detected at 492 nm with 4 nm slits in the presence of 100 μM ThT. At the end of the reaction, excitation scans were performed from 260 to 470 nm. For analytical ultracentrifugation, oligomerization was allowed to proceed for ~ 6 h prior to analysis.

Analytical Ultracentrifugation. All analytical ultracentrifugation experiments were performed on Beckman Xl-I analytical ultracentrifuge using an An-60 Ti analytical rotor. Sedimentation velocity was performed at 35 k rpm at 20 °C except for all H51 mutants, which were spun at 55 k rpm. Once loaded into the rotor, samples were thermally equilibrated for an additional 2−3 h prior to acquiring radial scans for ~15 h at 295 nm. Data analysis was performed using SedFit 94 assuming a spherical shape and using a c(s) distribution model (*37*). Sedimentation equilibrium was conducted at 20 °C at 15, 25, 35, 40, 45, 55, 65, 75, 90, and 100 μM protein at 8 k, 14 k, 18 k, 26 k, and 34 k rpm using a six channel cell. Samples were equilibrated at 20 °C for at least 15 h at each speed. Data was collected at 280 nm wavelength. A total of 38 sets of data were globally fit and confidence interval determined using HeteroAnalysis (*38*). Only three of these data sets are displayed in Figure 2.

Stability and Binding. Intrinsic fluorescence was monitored by excitation at 283 nm and emission scanned from 300 to 450 nm

with 2 nm slits at 25 °C. Protein concentration was 2.5 μM, in 25 mM MOPS, 200 mM potassium acetate, pH 7.4. Various amounts of competitive chelator, glycine, as well as ligand, copper acetate, were also present in the binding experiments as previously described (*34*). For chemical denaturation experiments, varying amounts of urea was added and all samples were incubated a minimum of 12 h prior to measurement. Not all constructs yielded data of sufficient quality to make confident the determination of stability and m-values (*39*). Fits were therefore used only to determine denaturation midpoints, (C_m).

Calculations. All binding and stability fits were performed using Mathematica 5.2 (*40*). Fluorescence intensities were measured by excitation at 283 nm with emission spectra collected from 300 to 450 nm. The intensity weighted average wavelength (AEW) was used as an order parameter for assessing unfolding to folding transitions (*41*). For β2m constructs these shifts range from 10 to 18 nm. For clarity, AEW order parameters are expressed in a renormalized form with 0 representing the AEW at 0 urea, and 1, the AEW at the highest concentration of urea used for a given construct. For determination of Cu^{2+} binding, global analysis was used to simultaneously fit Cu^{2+} titrations performed at five different concentration of the competitive chelate, glycine (*34*). Confidence intervals for global fits were performed using Monte Carlo analysis. All other error represents ± 1 standard deviation from ≥3 repeat experiments. Molecular graphics and rmsd calculations were done using PyMol (*42*). For rmsd calculations, structure alignments were made using Superpose (*43*) within ccp4 (*44*) . Chain A of 2F8O and 3CIQ and chain B of 2CLR were used in those calculations and residues 7−11, 22−27, 37−41, 65−68, 78−82, 89−94 for the structural alignment.

RESULTS

Oligomerization of β2m involves formation of intermediates that have undergone significant conformational rearrangements. Here, we induce the formation of the *trans* conformation at residue 32 using the previously characterized mutation P32A and assess its behavior in the holo state. The additional residues most likely associated with metal cation induced conformational change are the imidzole side chains at 13, 31, 51, and 84 (Figure 1). The effects of mutations at these locations are assessed on the background of P32A. This allows us to elucidate the role of the imidazole side chains in an activated, preamyloidogenic configuration approximated by P32A. Unless stated otherwise, all histidine mutants on the P32A background will be referred to by the single histidine mutation. For example, the double mutant H51FP32A will be referred to here as H51F.

P32A forms an oligomer population of a homogeneous size in response to metal binding. Sedimentation equilibrium analytical ultracentrifugation (AUC_{eq}) was performed on P32A at a range of concentration up to 100 μM protein and 200 μM Cu^{2+} in the presence of 0.5 M urea at pH 7.4, 20 °C. The presence of 0.5 M urea is not required for oligomerization (Supporting Information, Figure 1); rather it permits a more extensive comparison with our previously published work (*29*, *34*, *45*). Under these conditions, global analysis of 38 data sets reveals that P32A is most consistent with a tetrameric species in equilbrium with monomer (Figure 2). The equilibrium constant for this fit is 1.1×10^{14} M^{-3}, yielding an apparent $\Delta G°$ of −20 kJ/mol/subunit.

Cu^{2+}-induced oligomerization of P32A involves contacts mediated by His 51. Oligomerization of P32A was measured

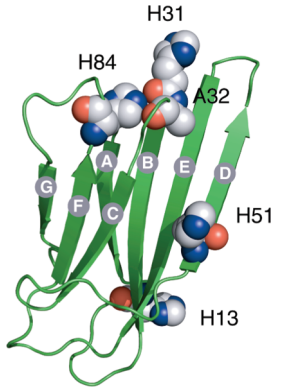

FIGURE 1: Ribbon representation of P32A (PDB ID: 2F8O). The strands are marked with established nomenclature A−G. Each of the four histidines and residue 32 are shown as spheres.

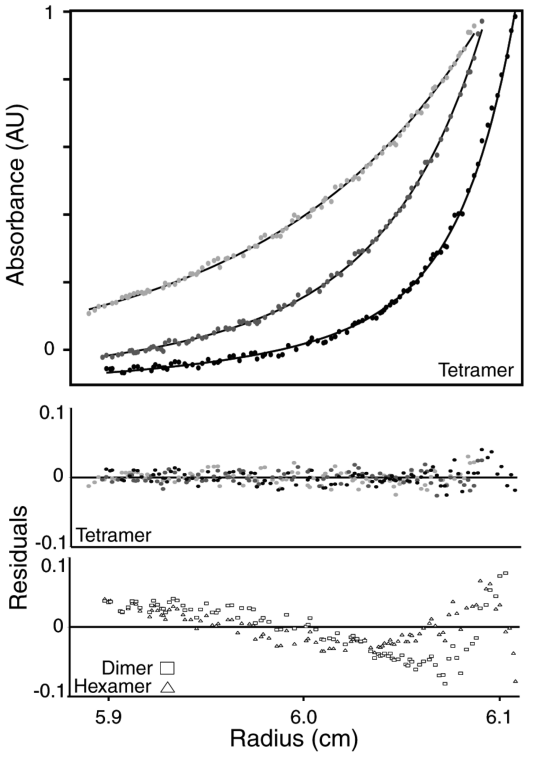

FIGURE 2: $P32A_{holo}$ is tetrameric. Sedimentation equilibrium analytical ultracentrifugation analysis of P32A is shown in the upper panel with a portion (3 of 38) of the global fit to a monomer−tetramer equilibrium. Traces shown are 25 μM P32A with 200 μM Cu^{2+} at 18 k (light gray), 26 k (dark gray), 34 k (black) rpm with protein absorbance plotted as a function of radial position. Middle panel displays residuals of fits shown above. Bottom panel displays residuals of fits for 34 k rpm trace to monomer−dimer (square) and monomer−hexamer (triangle) equilibrium, respectively.

under standard conditions by sedimentation velocity analytical ultracentrifugation (AUC_{sv}) for a range of β2m mutants lacking one of the four histidines present in the protein (Figure 3). Oligomerization profiles were also determined by size exclusion chromatography (SEC) (not shown) and are in good agreement with the AUC_{sv} data (Figure 3). Histidine residues were mutated to phenylalanine to conserve the size of the side chain. The exceptions to this were H84 and H31. Previous studies showed H84 to be intolerant of phenylalanine on a wild type background (*32*). In that work, H31 could be mutated to a phenylalanine; however here, on a P32A background, H31F could not be

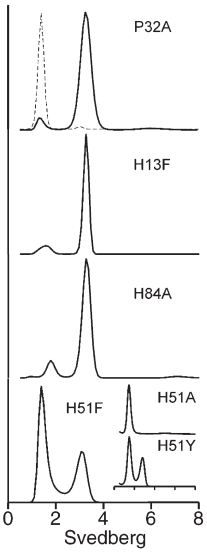

FIGURE 3: Oligomerization profiles of P32A and indicated double mutants in the presence of Cu^{2+}. Sedimentation velocity ultracentrifugation profiles are shown at 100 μM protein and 200 μM Cu^{2+} (solid line), except for the H51 mutants which show only the soluble fraction (~75 μM protein retained, as determined by UV-absorbance). Additionally, the profile of P32A is shown in the presence of 10 mM EDTA (dotted line, top panel). In the presence of EDTA, all double mutants give profiles which are comparable to each other and to that of P32A (not shown).

refolded. At near stoichiometric conditions, in the presence of Cu^{2+}, P32A forms 92 ± 1% oligomer. Under matched conditions, H13F and H84A behave similarly forming 86 ± 1% and 84 ± 5% oligomer, respectively. In contrast, oligomer formation by H51F is reduced, with only 32 ± 9% of the protein forming oligomers (Figure 3). H31A could not be analyzed under these conditions as all the protein precipitated in response to Cu^{2+} exposure. To complete our probe of the role of H51 in cation-mediated oligomerization, the imidazole was also mutated to tyrosine and alanine. For both constructs, oligomerization was strongly diminished to < 5% oligomer for H51A and 37 ± 3% for H51Y (Figure 3 inset). Taken together, these data suggest that His51 is an interface residue that mediates an intersubunit contact within the P32A β2m tetramer.

The affinity of P32A for Cu^{2+} is abrogated by mutation of H31. Copper affinities for P32A constructs were measured as previously described (*34*) (Figure 4A,C). As the affinities are much lower than the protein concentration required for fluorescence detection, a competition based assay was used (Figure 4C). The apparent affinity for P32A by this method is K_{d_app} = 0.6 nM, which is comparable to our previously reported value of 0.5 nM. Mutations at His84, His51, or His13 show no significant change in apparent affinity (Figure 4D). In marked contrast, the K_{d_app} of H31A could not be measured as changes in average emission wavelength (AEW) were no longer apparent (Figure 4B,C). Loss of fluorescence intensity was observed, but without evidence of a saturable binding isotherm. Loss in intensity could be caused by binding an alternative conformation in which one or both of the tryptophans are quenched. These observations clearly point to H31 as the central residue for metal binding in P32A.

Native state Cu^{2+} binding at H31 is further supported by a change in the kinetics of oligomerization with respect to those of P32A. The kinetics of oligomerization were obtained by monitoring the fluorescence change of an exogenous dye, ThT, upon

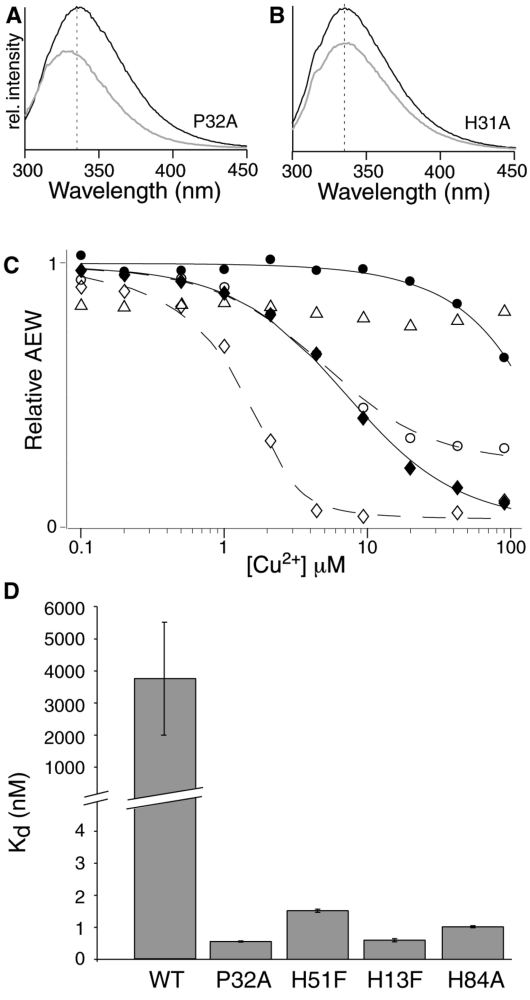

FIGURE 4: Cu^{2+} binding affinity of WT, P32A, and double mutants. Intrinsic fluorescence emission spectrum of 2.5 μM P32A (A) and 2.5 μM H31A (B) in the presence of 0 μM (black) or 45 μM Cu^{2+} (gray). Dotted line shows emission maximum in the absence of Cu^{2+}. (C) Average emission wavelength (*41*) as a function of Cu^{2+} concentration is plotted for WT (circle), P32A (diamond), and H31A (triangle). Data sets are shown in the presence (filled) and absence (open) of 370 μM glycine. (D) Affinity was measured from fits to the changes in intrinsic fluorescence upon titration with Cu^{2+}. For P32A and double mutants, affinity was determined by global analysis of five titrations prepared in the presence of a competitive chelate, glycine (*34*). No affinity could be measured for H31A by this method (B); see main text.

binding to β2m (*29*). All double mutants form oligomers within the dead time of the measurement (~2 min) with the exception of H31A (Figure 5). For H31A, addition of 2-fold excess of Cu^{2+} gives an initial rise in the ThT intensity that is visible for about 30 min, followed by a rapid drop in intensity associated with the formation of a visible precipitate (Figure 5). In experiments for which Cu^{2+}: protein ratios were substoichiometric, time dependent change in ThT fluorescence intensity is minimal and precipitate formation is absent (not shown). Under these conditions, H31A forms a negligible amount of oligomers over the hours time scale (AUC and SEC data not shown). Such a drastic change in the rate and efficiency of oligomer formation suggests a different mechanism of assembly, one that is dominated by the formation of amorphous precipitate. This aggregation pathway is likely governed by a different set of interactions with Cu^{2+} than that seen in P32A or any of the other mutants for which the native binding site at H31 is intact.

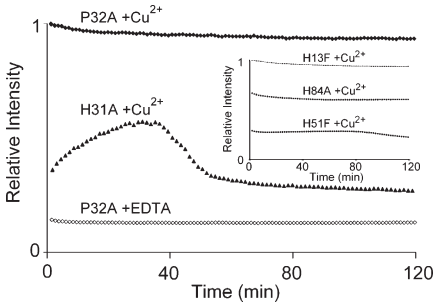

FIGURE 5: Oligomerization kinetics of P32A and double mutants. Kinetics of P32A (diamond) and H31A (triangle) were monitored by measuring the relative change in fluorescence intensity of ThT after the addition of Cu^{2+}. All reactions contained 100 μM β2m, 200 μM Cu^{2+} with 0.5 M urea and 100 μM ThT. Spectra were collected at 37 °C. The oligomerization kinetics of H13F, H84A, and H51F in the presence of Cu^{2+} were closely similar to P32A (inset).

Table 1: Urea Denaturation Midpoints for P32A and Double Mutants

	$C_{m\ apo}$ [a]	$C_{m\ holo}$ [b]
WT	5.7 ± 0.1	3.5 ± 0.2
P32A	4.4 ± 0.1	3.7 ± 0.2
H13F	5.0 ± 0.1	5.2 ± 0.3
H31A	4.4 ± 0.1	ND[c]
H51F	5.2 ± 0.1	4.9 ± 0.1
H84A	4.1 ± 0.1	4.1 ± 0.2

[a] Urea denaturation studies of 2.5 μM P32A and double mutants in the absence (apo) of 90 μM Cu^{2+}. These were measured at 25 °C and are reported as the C_m (i.e., denaturation midpoints) with units of (M). [b] Urea denaturation studies of 2.5 μM P32A and double mutants in the presence (holo) of 90 μM Cu^{2+}. These were measured at 25 °C and are reported as the C_m (i.e., denaturation midpoints) with units of (M). [c] ND, not determinable (see text).

The absence of an imidazole at residue 31 results in Cu^{2+}-induced destabilization. To monitor the apparent stability of our constructs, urea denaturation studies were performed. In the presence of 36-fold excess Cu^{2+}, P32A shows a shift in its C_m of ~0.7 M (Table 1). We previously noted that high molar excess of Cu^{2+} could result in destabilization of WT protein (*32*). Here, the C_m for WT shifts ~2.2 M (Table 1). Binding that is accompanied by destabilization necessarily requires a binding site to be present in non-native conformations of the protein. This effect is diminished for P32A relative to WT, most likely a result of the fact that the folded state affinity of P32A for Cu^{2+} is much greater (*34*). In contrast to the P32A background construct, the double mutants H13F, H51F, and H84A show C_m values in the presence of Cu^{2+} that are closely similar to their respective apo forms (Table 1). This is comparable to previous observations of WT protein where H13, H51, and H84 were identified as participants in non-native state Cu^{2+} binding. Here, under the same conditions, it is remarkable that the double mutant H31A unfolds in response to titration with Cu^{2+}. At a reduced stoichiometry, 6:1 Cu^{2+}/protein, H31A has a C_m value of 3.6 M relative to the apo form of 4.4 M, a difference of 0.8 M. At 15-fold excess Cu^{2+}, this difference increases to 1.7 M (Figure 6). At the latter of these Cu^{2+}/protein molar ratios, the stability of P32A still remains within error of the apo protein (Figure 6). These results suggest that P32A not only possesses a native Cu^{2+} binding site at H31 but also retains properties of the non-native binding site we previously reported for the WT protein (*32*). Once H31 is removed by mutation, the protein can no longer bind Cu^{2+} as efficiently in its native state yet continues to bind Cu^{2+} in the non-native conformation. This manifests itself in H31A as Cu^{2+}-induced unfolding.

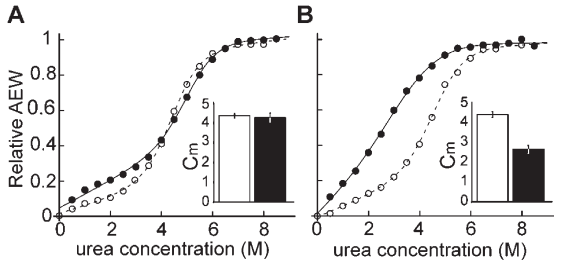

FIGURE 6: Stability of P32A and H31A. Representative urea denaturation curves of 2.5 μM P32A (A) and H31A (B) in the absence (open) and presence (solid) of 15-fold excess Cu^{2+}. The folded state of the constructs was monitored using intrinsic fluorescence and expressed as relative average emission wavelength (see Calculations in Experimental Procedures). Inset shows the average C_m value determined from the fits.

DISCUSSION

In the β2m system, non-prolyl mutants of the *cis* P32 residue represent a species of known structure that is predominantly monomeric but is predisposed to form amyloid and amyloidogenic species (*7*, *16*, *18*, *34*, *35*, *46*). Here we assess the histidine residues on the P32A background to enhance our understanding of the structural basis of metal induced oligomerization of β2m. We observe several notable behaviors: (i) Oligomers of $P32A_{holo}$ are tetrameric. (ii) H51 is a critical residue in mediating an oligomeric interface. (iii) Oligomerization is not coupled to strong (nM) Cu^{2+} binding affinity. (iv) The side chain of H31 is critical to Cu^{2+} binding by the P32A folded state. (v) A secondary binding site and non-native form of β2m is apparent upon copper binding to P32A in the absence of the H31 side chain. Below, our findings are discussed with respect to the known apo and holo structures of β2m.

P32A, like WT protein, oligomerizes in a ligand-dependent manner. In WT, dimer, tetramer, and hexameric species are observed (*29*). Our recent structural work suggests that dimer and tetramer are intermediates to a stable hexamer (*30*). In contrast, P32A in the presence of Cu^{2+} forms a stable tetramer. The basis for this difference is a combination of structural and energetic effects. A particularly significant energetic difference is illuminated by the ~ 6000 fold increase in Cu^{2+} binding affinity of P32A relative to WT. In this work, we note that only mutation of H31 results in loss of affinity. This is consistent with previous work (*30*, *32*) and suggests that increased affinity can be mapped to the energetic cost of an altered loop structure that includes a *trans*-peptide bond at residue 32. For P32A, mutation predisposes the BC loop to form its metal binding conformation (Figure 8A,B and Table 2). In addition, a significant structural difference is illuminated by the observation that H13 on a WT background strongly affects oligomerization (*30*), whereas here, on the background of P32A, the effect is substantially diminished (Figure 3). One reason for this could be that H13 plays a structurally different role in the WT and P32A interfaces. Alternatively, the energetic contribution of H13 as an interface residue in WT and P32A may be distinct. Insight into the range of possibilities that account for these differences are evident in comparisons of the known crystal structures of β2m.

The interfaces present in tetrameric $P32A_{holo}$ are necessarily distinct from those present in the holo hexameric state, $H13F^{WT}_{holo}$. To be clear, $H13F^{WT}_{holo}$ refers to a point mutation on a wild type

Table 2: Structural Differences of β2m Variants

region[a]	$H13F^{WT}_{holo}-WT_{apo}$[a]b	$P32A_{apo}-WT_{apo}$[a]c	$P32A_{apo}-H13F^{WT}_{holo}$[a]d
A strand 0−6	2.8/4.1	N/A/N/A[e]	N/A/N/A
BC loop 29−34	2.8/4.1	2.6/4.2	1.7/2.1
D strand 52−55	0.8/1.1	2.3/4.2	2.0/4.1
DE loop 56−63	3.2/4.3	3.7/5.0	1.9/3.2

[a] Regions of β2m defined by inspection of structure (Figure 1) and backbone Cα rmsd (Figure 8). rmsd's are reported as pairs, $<C\alpha>$ / <all atoms>, for comparisons of [b]$H13F^{WT}_{holo}$ (PDB ID: 3CIQ (*30*)) with WT_{apo} (PDB ID: 2CLR (*54*)), [c]$P32A_{apo}$ (PDB ID: 2F8O (*34*)) with WT_{apo}, and [d]$P32A_{apo}$ with $H13F^{WT}_{holo}$. All rmsd values are reported in (Å). [e] N/A, not applicable.

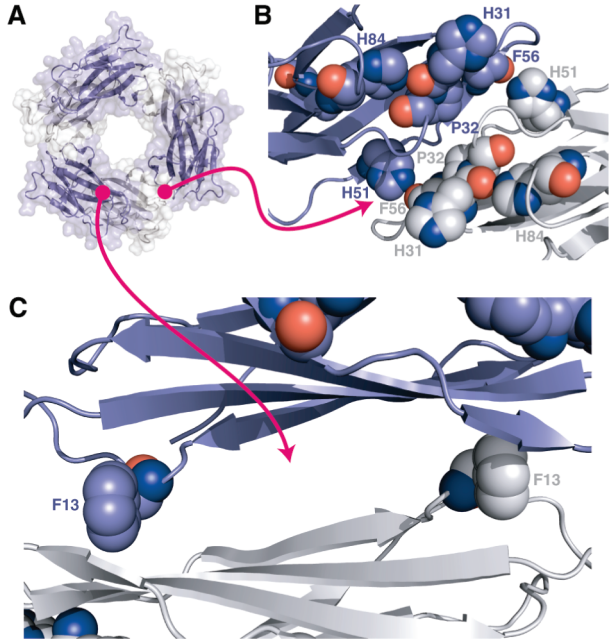

FIGURE 7: Interfaces formed by hexameric $\beta2m_{holo}$. (A) Ribbon representation of the $H13F^{WT}_{holo}$ hexamer (PDB ID: 3CIQ (*30*)) viewed down the 3-fold symmetry axis with the subunits alternately colored white and blue. Close up of the D:D intrasheet interface (B) and the ABED/ABED intersheet interface (C) showing residues 13, 31, 32, 51, and 84 and the backbone of residue 56 as space filled.

and not a P32A background. The differences that give rise to tetrameric vs hexameric states could be the result of entirely unique interfaces. Alternatively, a subset of interactions apparent in the structure of $H13F^{WT}_{holo}$ could be present in $P32A_{holo}$. Two interfaces are present in the $H13F^{WT}_{holo}$ hexamer (Figure 7A). The first consists of contacts formed predominantly by interactions of two adjacent D strands, each contributed by one monomer of β2m (Figure 7B). The second is formed by the stacking of two ABED sheets from adjacent monomers onto one another (Figure 7C). Across this ABED/ABED intersheet interface of $H13F^{WT}_{holo}$, residue 13 makes a significant contact supported by the fact that its mutation to an alanine results in strong reduction of oligomerization. In contrast, residue 13 does not play an important role in oligomerization of $P32A_{holo}$. Neither mutation to phenylalanine (Figure 3), nor alanine (not shown), appreciably affects oligomerization under the conditions used here. This suggests that the ABED/ABED interface evident in $H13F^{WT}_{holo}$ is not precisely mirrored in the $P32A_{holo}$ tetramer. Across the D:D strand/strand interface of $H13F^{WT}_{holo}$, the side chain of H51 forms a hydrogen bond with the backbone of F56 of an adjacent subunit. It is also central in $P32A_{holo}$, as mutation of H51 results in a dramatic decrease in oligomerization (Figure 3). Since mutation of H51 does not significantly reduce folded stability (Table 1), this observation is most consistent with H51 participating in an interface. Importantly, in $P32A_{apo}$, the side chain of H51 does not appear to make any significant intermolecular contacts and could not participate in the same interaction across an interstrand interface if we assume that the conformationally distinct strand D in $P32A_{apo}$ is retained in $P32A_{holo}$. This suggests that if a D-strand mediated interface is present in $P32A_{holo}$, then it more likely resembles that seen in $H13F^{WT}_{holo}$ than that seen in $P32A_{apo}$. Taken together, this data suggests that if one and only one of the interfaces of $H13F^{WT}_{holo}$ is retained in $P32A_{holo}$, it is more likely to be the D:D strand to strand interface.

The copper-dependent oligomers described here undergo subsequent, noncovalent alterations to form irreversible, metal cation independent oligomeric species (*45*). We believe such alterations to be critical to the formation of aggregates that are stable *in vivo*. We conjecture that such changes result from alternative assemblies based on interfaces that are similar but not identical to atomic structures already characterized. One indication of what such a change might include in $P32A_{holo}$ is evident in the plasticity of the D-strand. Solution NMR data suggests the D strand of β2m to be dynamic, dominated by two short β-strand segments separated by a β-bulge at residue D53 (*47*, *48*). This is the only form of strand D evident for β2m in complex with class I MHC crystal structures. Conformational dynamics, however, appear reflected in two alternative, bulge-free conformations of the D-strand. These are evident crystallographically in WT_{apo}, (PDB ID: 1LDS) and $P32A_{apo}$ (PDB ID: 2F8O) (*34*, *48*−*51*). In the latter case, a 180° rotation of the backbone and a register shift is observed for β-strand residues C-terminal to residue 53, while in the former, the rotation and shift are N-terminal (Figure 8C). Conformational variability in strand D also extends into the DE loop of the protein, as is the case for P32A (Figure 8A and Table 2), monomeric WT (*48*), and several DE loop mutants (*34*, *48*, *50*, *51*). Therefore, it is likely that any changes impacting strand D would also affect the DE loop, which has also been suggested to be important in β2m aggregation (*50*, *51*).

The loss of a β-bulge in strand D has been suggested as a possible origin for mediating subsequent, irreversible assembly (*48*). In our structure of $P32A_{apo}$, we observe one possible mode for such an interaction. This involves D:D contacts across a crystallographic dimer. Importantly, this state is not readily sampled in dilute solution but rather dominates only under high protein concentrations associated with crystallization. Thus, the D:D strand contact of $P32A_{apo}$ likely represents a higher energy conformation than the one observed in hexameric β2m. We conjecture that the conformations of β2m that are oligomeric, irreversible, and metal free (*26*, *45*) may result from sampling the higher energy D:D strand interface evident in the crystal structure of $P32A_{apo}$. Plasticity in β strands has been reported in functional classes of protein−protein interactions. For example, the PAS-B

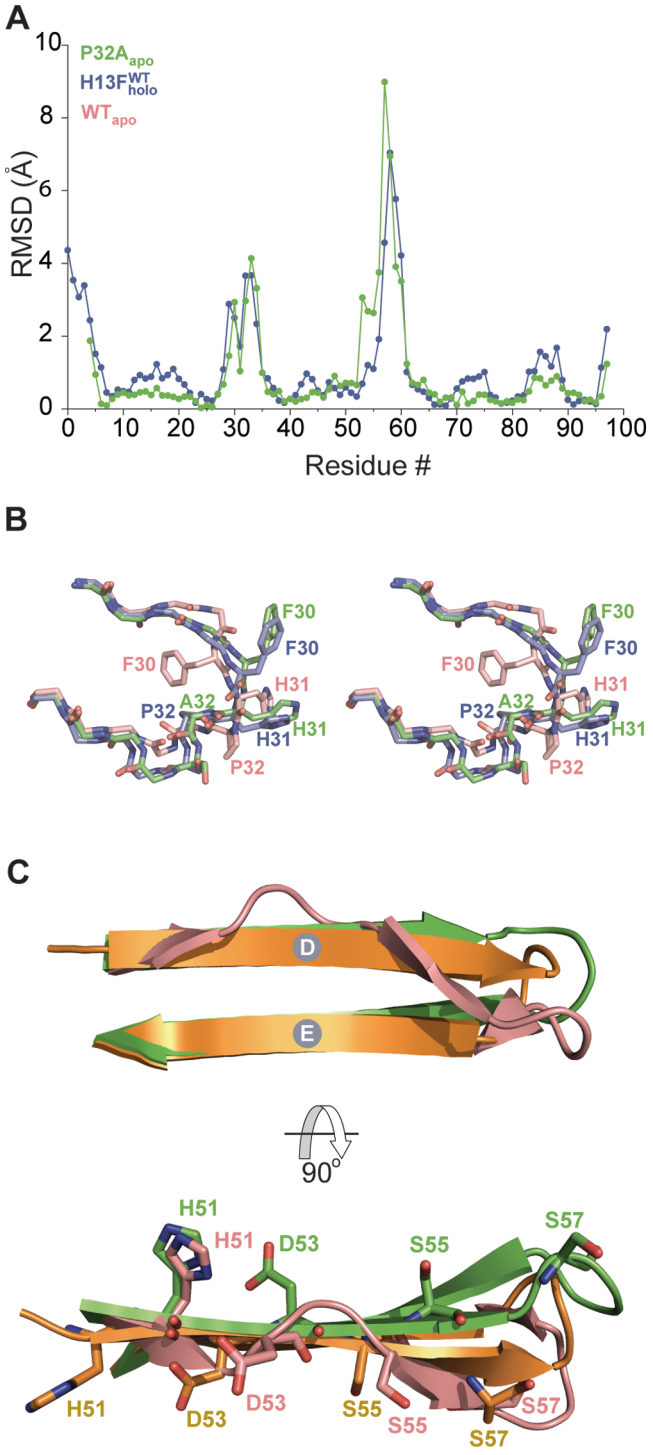

FIGURE 8: Comparison of alternative structural elements sampled by β2m. (A) Structural differences of P32A$_{apo}$ (PDB ID: 2F8O) and H13F$^{WT}_{holo}$(PDB ID: 3CIQ) relative to WT$_{apo}$ (PDB ID: 2CLR (*54*)). rmsd values are plotted on a per residue basis as calculated for backbone Cα. (B) Overlay of the BC loops of P32A$_{apo}$ (green), H13F$^{WT}_{holo}$ (blue), and WT$_{apo}$ (salmon) (PDB ID: 2CLR) shown as cross-eyed stereo pairs. Main chain is shown as sticks with side chains drawn only for residues 30−33. (C) Overlay of three alternative conformations of strands D and E (residues 50−67). The view shown in the direction of the D strand edge (lower) additionally shows the main and side chains of residues 51, 53, 55, and 57 as sticks. Structures used in this figure are P32A$_{apo}$ (green), WT$_{apo}$ (orange) (PDB ID: 1LDS (*48*)), and WT$_{apo}$ taken from its complex with class I MHC (PDB ID: 2CLR).

interaction domain of the aryl hydrocarbon receptor nuclear translocator readily samples alternate registrations in one of its β strands. These translate to flexibility in a solvent exposed β sheet surface that is involved in complex formation (*52*). Thus, β strand plasticity may be an intrinsic property of β-sheets that can serve both pathological and functional roles.

High energy states accessible to native proteins are transiently sampled and may represent aggregation-prone species (*7*). Such states may be characterized as alternative conformers, or locally unfolded states termed N*. As such, they may increase the solvent accessibility of normally buried, hydrophobic residues. In the case of P32A$_{apo}$ as well as in H13F$^{WT}_{holo}$, residue F30 is a prominent example of a normally buried residue that becomes solvent accessible and involved in an interface. Thermal fluctuations have been suggested as one mechanism for crossing the energy barrier to access N* (*7*). It is equally plausible that ligand binding energy may serve as an alternative means of accessing N* states. For β2m, as well as in other systems such as PrP (*53*), liganded and nonliganded sources of fluctuations appear to simply be variants of a common assembly pathway (*30*, *46*). P32A$_{apo}$ is less stable than WT and has captured some, but perhaps not all of the characteristics that β2m's N* state requires for self-association. Elucidating the subtle structural changes leading to higher energy states and self-association is important to better understanding the factors that give rise to amyloid formation. This can serve not only in detecting biomedically relevant targets for diagnosis, but also in designing functional therapeutics to treat such ailments.

ACKNOWLEDGMENT

We thank D. Engelman and A. Schepartz, E. Matthews and C. Craig for assistance with analytical ultracentrifugation and L. Regan, M. Calabrese for helpful discussions. We are also grateful to M. Calabrese and A. Nath for careful reading of this manuscript.

SUPPORTING INFORMATION AVAILABLE

Sedimentation equilibrium data of P32A$_{holo}$ in the absence of urea (Supplementary Figure 1) and near UV CD spectra of WT, P32A, and P32A double mutants with experimental procedures (Supplementary Figure 2) is available free of charge via the Internet at http://pubs.acs.org.

REFERENCES

1. Chiti, F., and Dobson, C. M. (2006) Protein misfolding, functional amyloid, and human disease. *Annu. Rev. Biochem. 75*, 333–366.
2. Selkoe, D. J. (2003) Folding proteins in fatal ways. *Nature 426*, 900–904.
3. Pepys, M. B. (2006) Amyloidosis. *Annu. Rev. Med. 57*, 223–241.
4. Tycko, R. (2004) Progress towards a molecular-level structural understanding of amyloid fibrils. *Curr. Opin. Struct. Biol. 14*, 96–103.
5. Dobson, C. M. (2002) Getting out of shape. *Nature 418*, 729–730.
6. Fandrich, M., Fletcher, M. A., and Dobson, C. M. (2001) Amyloid fibrils from muscle myoglobin. *Nature 410*, 165–166.
7. Chiti, F., and Dobson, C. M. (2009) Amyloid formation by globular proteins under native conditions. *Nat. Chem. Biol. 5*, 15–22.
8. Wearsch, P. A., and Cresswell, P. (2008) The quality control of MHC class I peptide loading. *Curr. Opin. Cell Biol. 20*, 624–631.
9. Floege, J., and Ehlerding, G. (1996) Beta-2-microglobulin-associated amyloidosis. *Nephron 72*, 9–26.
10. Menaa, C., Esser, E., and Sprague, S. M. (2008) Beta2-microglobulin stimulates osteoclast formation. *Kidney Int. 73*, 1275–1281.
11. Drueke, T. B. (2000) Beta2-microglobulin and amyloidosis. *Nephrol. Dial. Transplant. 15*, 17–24.
12. Malaguarnera, M., Restuccia, S., Di Fazio, I., Zoccolo, A. M., Trovato, B. A., and Pistone, G. (1997) Serum beta2-microglobulin in chronic hepatitis C. *Dig. Dis. Sci. 42*, 762–766.

13. Keating, M. J. (1999) Chronic lymphocytic leukemia. *Semin. Oncol. 26*, 107–114.
14. Morgan, C. J., Gelfand, M., Atreya, C., and Miranker, A. D. (2001) Kidney dialysis-associated amyloidosis: a molecular role for copper in fiber formation. *J. Mol. Biol. 309*, 339–345.
15. Okon, M., Bray, P., and Vucelic, D. (1992) 1H NMR assignments and secondary structure of human beta 2-microglobulin in solution. *Biochemistry 31*, 8906–8915.
16. Jahn, T. R., Parker, M. J., Homans, S. W., and Radford, S. E. (2006) Amyloid formation under physiological conditions proceeds via a native-like folding intermediate. *Nat. Struct. Mol. Biol. 13*, 195–201.
17. Chiti, F., Mangione, P., Andreola, A., Giorgetti, S., Stefani, M., Dobson, C. M., Bellotti, V., and Taddei, N. (2001) Detection of two partially structured species in the folding process of the amyloidogenic protein beta 2-microglobulin. *J. Mol. Biol. 307*, 379–391.
18. Kameda, A., Hoshino, M., Higurashi, T., Takahashi, S., Naiki, H., and Goto, Y. (2005) Nuclear magnetic resonance characterization of the refolding intermediate of beta(2)-microglobulin trapped by non-native prolyl peptide bond. *J. Mol. Biol. 348*, 383–397.
19. McParland, V. J., Kad, N. M., Kalverda, A. P., Brown, A., Kirwin-Jones, P., Hunter, M. G., Sunde, M., and Radford, S. E. (2000) Partially unfolded states of beta(2)-microglobulin and amyloid formation in vitro. *Biochemistry 39*, 8735–8746.
20. Esposito, G., Michelutti, R., Verdone, G., Viglino, P., Hernandez, H., Robinson, C. V., Amoresano, A., Dal Piaz, F., Monti, M., Pucci, P., Mangione, P., Stoppini, M., Merlini, G., Ferri, G., and Bellotti, V. (2000) Removal of the N-terminal hexapeptide from human beta 2-microglobulin facilitates protein aggregation and fibril formation. *Protein Sci. 9*, 831–845.
21. Yamamoto, S., Hasegawa, K., Yamaguchi, I., Tsutsumi, S., Kardos, J., Goto, Y., Gejyo, F., and Naiki, H. (2004) Low concentrations of sodium dodecyl sulfate induce the extension of beta 2-microglobulin-related amyloid fibrils at a neutral pH. *Biochemistry 43*, 11075–11082.
22. Yamamoto, S., Yamaguchi, I., Hasegawa, K., Tsutsumi, S., Goto, Y., Gejyo, F., and Naiki, H. (2004) Glycosaminoglycans enhance the trifluoroethanol-induced extension of beta 2-microglobulin-related amyloid fibrils at a neutral pH. *J. Am. Soc. Nephrol. 15*, 126–133.
23. Sasahara, K., Yagi, H., Naiki, H., and Goto, Y. (2007) Heat-induced conversion of beta(2)-microglobulin and hen egg-white lysozyme into amyloid fibrils. *J. Mol. Biol. 372*, 981–991.
24. Myers, S. L., Jones, S., Jahn, T. R., Morten, I. J., Tennent, G. A., Hewitt, E. W., and Radford, S. E. (2006) A systematic study of the effect of physiological factors on beta2-microglobulin amyloid formation at neutral pH. *Biochemistry 45*, 2311–2321.
25. Linse, S., Cabaleiro-Lago, C., Xue, W. F., Lynch, I., Lindman, S., Thulin, E., Radford, S. E., and Dawson, K. A. (2007) Nucleation of protein fibrillation by nanoparticles. *Proc. Natl. Acad. Sci. U.S.A. 104*, 8691–8696.
26. Antwi, K., Mahar, M., Srikanth, R., Olbris, M. R., Tyson, J. F., and Vachet, R. W. (2008) Cu(II) organizes beta-2-microglobulin oligomers but is released upon amyloid formation. *Protein Sci. 17*, 748–759.
27. Barnham, K. J., and Bush, A. I. (2008) Metals in Alzheimer's and Parkinson's diseases. *Curr. Opin. Chem. Biol. 12*, 222–228.
28. Viles, J. H., Klewpatinond, M., and Nadal, R. C. (2008) Copper and the structural biology of the prion protein. *Biochem. Soc. Trans. 36*, 1288–1292.
29. Eakin, C. M., Attenello, F. J., Morgan, C. J., and Miranker, A. D. (2004) Oligomeric assembly of native-like precursors precedes amyloid formation by beta-2 microglobulin. *Biochemistry 43*, 7808–7815.
30. Calabrese, M. F., Eakin, C. M., Wang, J. M., and Miranker, A. D. (2008) A regulatable switch mediates self-association in an immunoglobulin fold. *Nat. Struct. Mol. Biol. 15*, 965–971.
31. Esposito, G., Corazza, A., Viglino, P., Verdone, G., Pettirossi, F., Fogolari, F., Makek, A., Giorgetti, S., Mangione, P., Stoppini, M., and Bellotti, V. (2005) Solution structure of beta(2)-microglobulin and insights into fibrillogenesis. *Biochim. Biophys. Acta: Proteins Proteomics 1753*, 76–84.
32. Eakin, C. M., Knight, J. D., Morgan, C. J., Gelfand, M. A., and Miranker, A. D. (2002) Formation of a copper specific binding site in non-native states of beta-2-microglobulin. *Biochemistry 41*, 10646–10656.
33. Lim, J., and Vachet, R. W. (2004) Using mass spectrometry to study copper-protein binding under native and non-native conditions: beta-2-microglobulin. *Anal. Chem. 76*, 3498–3504.
34. Eakin, C. M., Berman, A. J., and Miranker, A. D. (2006) A native to amyloidogenic transition regulated by a backbone trigger. *Nat. Struct. Mol. Biol. 13*, 202–208.
35. Jahn, T. R., Tennent, G. A., and Radford, S. E. (2008) A common beta-sheet architecture underlies in vitro and in vivo beta2-microglobulin amyloid fibrils. *J. Biol. Chem. 283*, 17279–17286.
36. Levine, H. (1993) Thioflavine-T Interaction with synthetic Alzheimers-disease beta-amyloid peptides - detection of amyloid aggregation in solution. *Protein Sci. 2*, 404–410.
37. Schuck, P. (2000) Size-distribution analysis of macromolecules by sedimentation velocity ultracentrifugation and lamm equation modeling. *Biophys. J. 78*, 1606–1619.
38. Cole, J. L. (2004) Analysis of heterogeneous interactions. *Methods Enzymol. 384*, 212–232.
39. Bolen, D. W., and Santoro, M. M. (1988) Unfolding free energy changes determined by the linear extrapolation method. 2. Incorporation of delta G degrees N-U values in a thermodynamic cycle. *Biochemistry 27*, 8069–8074.
40. Wolfram Research, Inc. (2005), Champaign, IL.
41. Royer, C. A., Mann, C. J., and Matthews, C. R. (1993) Resolution of the fluorescence equilibrium unfolding profile of trp aporepressor using single tryptophan mutants. *Protein Sci. 2*, 1844–1852.
42. DeLano, W. L. (2002) DeLano Scientific, Palo Alto, CA, USA.
43. Krissinel, E., and Henrick, K. (2004) Secondary-structure matching (SSM), a new tool for fast protein structure alignment in three dimensions. *Acta Crystallogr. Sect. D Biol. Crystallogr. 60*, 2256–2268.
44. Collaborative Computational Project, Number 4 (1994) The CCP4 suite: programs for protein crystallography. *Acta Crystallogr. Sect. D Biol. Crystallogr. 50*, 760–763.
45. Calabrese, M. F., and Miranker, A. D. (2007) Formation of a stable oligomer of beta-2 microglobulin requires only transient encounter with Cu(II). *J. Mol. Biol. 367*, 1–7.
46. Eichner, T., and Radford, S. E. (2009) A generic mechanism of â2-microglobulin amyloid assembly at neutral pH involving a specific proline switch. *J. Mol. Biol. 386*, 1312–1326.
47. Verdone, G., Corazza, A., Viglino, P., Pettirossi, F., Giorgetti, S., Mangione, P., Andreola, A., Stoppini, M., Bellotti, V., and Esposito, G. (2002) The solution structure of human beta 2-microglobulin reveals the prodromes of its amyloid transition. *Protein Sci. 11*, 487–499.
48. Trinh, C. H., Smith, D. P., Kalverda, A. P., Phillips, S. E. V., and Radford, S. E. (2002) Crystal structure of monomeric human beta-2-microglobulin reveals clues to its amyloidogenic properties. *Proc. Natl. Acad. Sci. U.S.A. 99*, 9771–9776.
49. Iwata, K., Matsuura, T., Sakurai, K., Nakagawa, A., and Goto, Y. (2007) High-resolution crystal structure of beta(2)-microglobulin formed at pH 7.0. *J. Biochem. 142*, 413–419.
50. Esposito, G., Ricagno, S., Corazza, A., Rennella, E., Gumral, D., Mimmi, M. C., Betto, E., Pucillo, C. E., Fogolari, F., Viglino, P., Raimondi, S., Giorgetti, S., Bolognesi, B., Merlini, G., Stoppini, M., Bolognesi, M., and Bellotti, V. (2008) The controlling roles of Trp60 and Trp95 in beta2-microglobulin function, folding and amyloid aggregation properties. *J. Mol. Biol. 378*, 887–897.
51. Ricagno, S., Colombo, M., de Rosa, M., Sangiovanni, E., Giorgetti, S., Raimondi, S., Bellotti, V., and Bolognesi, M. (2008) DE loop mutations affect beta2-microglobulin stability and amyloid aggregation. *Biochem. Biophys. Res. Commun. 377*, 146–150.
52. Evans, M. R., Card, P. B., and Gardner, K. H. (2009) ARNT PAS-B has a fragile native state structure with an alternative {beta}-sheet register nearby in sequence space. *Proc. Natl. Acad. Sci. U. S. A. 106*, 2617–2622.
53. Calabrese, M. F., and Miranker, A. D. (2009) Metal binding sheds light on mechanisms of amyloid assembly. *Prion 3*, 1–4.
54. Collins, E. J., Garboczi, D. N., and Wiley, D. C. (1994) Three-dimensional structure of a peptide extending from one end of a class I MHC binding site. *Nature 371*, 626–629.